

Three-dimensional mesoscale dynamics of block copolymers under shear: The dynamic density-functional approach

A. V. Zvelindovsky, G. J. A. Sevink, B. A. C. van Vlimmeren, N. M. Maurits,
and J. G. E. M. Fraaije

Department of Biophysical Chemistry, University of Groningen, Nijenborgh 4, 9747 AG Groningen, The Netherlands

(Received 22 October 1997; revised manuscript received 2 February 1998)

Three-dimensional (3D) simulations of meso-phase formation in block copolymer melts under simple steady shear are performed in the framework of dynamic density-functional theory. The most stable “perpendicular” lamellar ordering is observed. The difference between 2D and 3D ordering in a model system is described. Lamellae reorientation and breakup are discussed. [S1063-651X(98)50505-3]

PACS number(s): 83.10.Nn, 64.70.Ja, 64.60.Ht, 82.20.Wt

Block copolymers are fascinating materials that are capable of forming mesoscale structures whose morphology can be tailored by controlled synthesis. It is known that flow fields affect these structures, giving rise to global orientation [1,2]. This is an intensively studied topic both experimentally and theoretically [3–5]. Especially the stability analysis of patterns and phase transitions in complex polymer liquids under shear have been studied intensively [2,6–10]. The lamellar alignment under shear has received much attention in small angle neutron scattering and x-ray scattering experiments [5,11–14]. During the last couple of years the time evolution of patterns in complex fluids in external flows has also been studied by computer simulation techniques using time dependent Landau-Ginzburg models [1,15–20]. These models are based on traditional free energy expansion methods (Cahn-Hilliard [21], Oono-Puri [22], and Flory-

Huggins-de Gennes [23]) which contain only the basic physics of phase separation [24] and are not well suited for specific application to the different complex industrial and biological liquids. In contrast to these phenomenological theories we do not truncate a free energy expansion, but rather retain the full polymer path integral by a numerical procedure [24–30]. Very recently Kawakatsu and Doi started to use a similar approach [31,32]. The benefit of such an approach is that it allows for the description of the mesoscopic dynamics of a *specific* complex polymer liquid [33].

The time evolution of morphologies in complex liquids under shear has been studied using Landau type free energies in 2D geometries such as a square cell [1,17,18,20], a rectangle [15,16] and in a two-dimensional Couette flow [15]. In recent fundamental work [31] the shear effect in a 2D polymer system has been studied using the path integral formalism for the kinetic coefficient. However, this was carried out for a model with simple periodic boundary conditions and a conventional phenomenological free energy. To our knowledge no simulations of polymer morphology formation in a 3D flow have been reported. Here we extend the dynamic density-functional method [25,26] to polymer liquids under simple shear flow.

The polymer melt is modeled as a compressible system, consisting of Gaussian chain molecules in a mean field environment. The free energy functional for copolymer melts has the form [26,27,33]

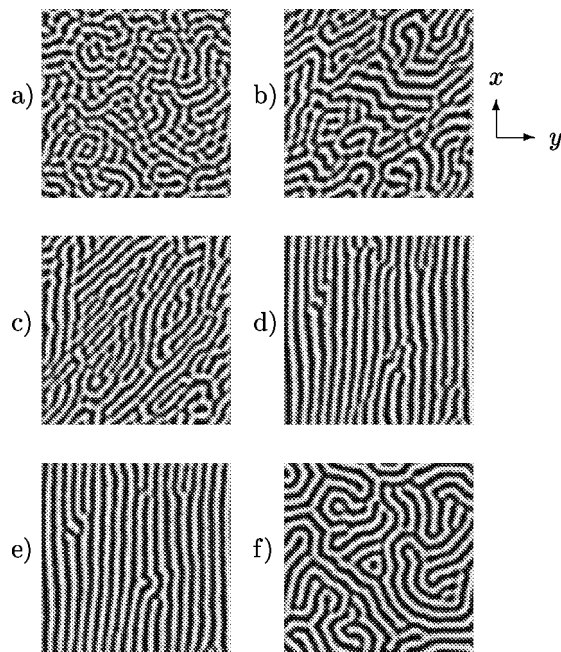


FIG. 1. Morphologies of A_8B_8 in 2D under shear: (a) $\tau=500$ (starting configuration for shear), (b) $\tau=1000$, (c) $\tau=2000$, (d) $\tau=4000$ (end shear), (e) $\tau=4500$ (from $\tau=4000$ to 4500 diffusion only). (f) is a reference picture at $\tau=4500$ for the morphology without any shear.

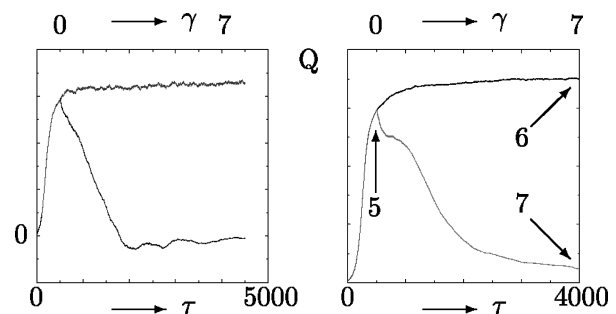


FIG. 2. Anisotropy factor Q (2D left and 3D right): diffusion only (top line) and with shear (bottom line). Shear is applied at $\tau=500$. The positions of the structures that are displayed in Figs. 5–7 are indicated. The shear strain γ is indicated on top of the figures.

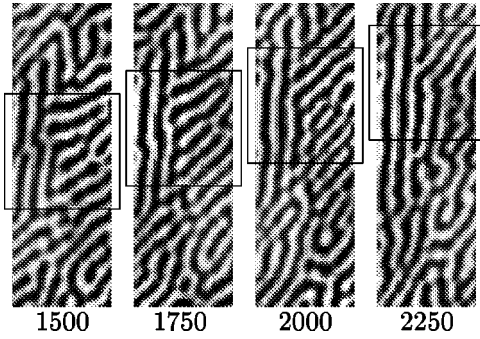


FIG. 3. Details of the reorientation mechanism by breaking up the lamellae as a function of time τ . The area of interest is in the middle of the picture at $\tau=1500$ and slowly moves in the direction of the shear.

$$\begin{aligned}
 F[\{\rho\}] = & -kT \ln \frac{\Phi^n}{n!} - \sum_I \int_V U_I(\mathbf{r}) \rho_I(\mathbf{r}) d\mathbf{r} \\
 & + \frac{1}{2} \sum_{I,J} \int_{V^2} \epsilon_{IJ}(\mathbf{r}-\mathbf{r}') \rho_I(\mathbf{r}) \rho_J(\mathbf{r}') d\mathbf{r} d\mathbf{r}' \\
 & + \frac{\kappa_H}{2} \int_V \left(\sum_I v_I [\rho_I(\mathbf{r}) - \rho_I^0] \right)^2 d\mathbf{r},
 \end{aligned}$$

where n is the number of polymer molecules, Φ is the intramolecular partition function for ideal Gaussian chains in an external field U , I is a component index, and V is the system volume. The external potentials U_I are conjugate to the densities ρ_I via the Gaussian chain density functional [26]. The average concentration is ρ_I^0 and v_I is the molecular volume of chain bead I . The cohesive interactions have kernels ϵ_{IJ} . The Helfand compressibility parameter is κ_H [27].

The time evolution of the density field $\rho_I(\mathbf{r})$ under simple shear flow, $v_x = \dot{\gamma}y$, $v_y = v_z = 0$, can be described by a time dependent Landau-Ginzburg type equation with a convective term [1,3,20]

$$\dot{\rho}_I = M_I \nabla \cdot \rho_I \nabla \frac{\delta F}{\delta \rho_I} - \dot{\gamma} y \nabla_x \rho_I + \eta_I. \quad (1)$$

M_I is a mobility parameter, $\dot{\gamma}$ is the shear rate (the time derivative of the strain γ), η_I is a stochastic term which is

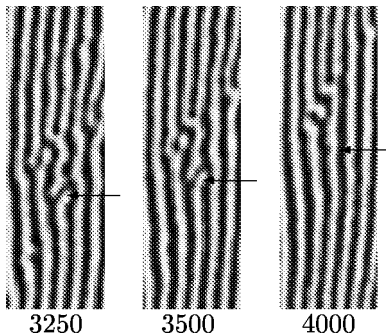


FIG. 4. Details of the defect annihilation under shear as a function of time τ . An example is indicated by the arrows.

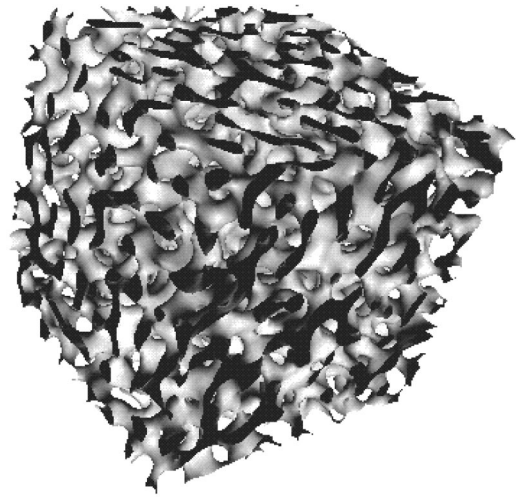


FIG. 5. Isosurface representation of the A_8B_8 melt at $\tau=500$ with diffusion only. The isosurface is $v_A \rho_A = 0.3$.

distributed according to the fluctuation-dissipation theorem [29]. For a $L \times L \times L$ cubic grid we use sheared periodic boundary conditions [34],

$$\rho(x, y, z, t) = \rho(x + iL + \gamma jL, y + jL, z + kL, t).$$

As an example, we simulate the behavior of a model polymer, which is represented by an A_8B_8 Gaussian chain. The dimensionless parameters that are used in the numerics are chosen as (see [26] and [33] for details) the dimensionless time step $\Delta\tau = \beta^{-1} M h^{-2} \Delta t = 0.5$, the grid parameter $d = ah^{-1} = 1.1543$, the noise scaling parameter Ω , which is related to mobility in Eq. (1), equals 100, the exchange parameter $\beta \epsilon_{AB} v^{-1} = 1.0$ ($\epsilon_{AA} = \epsilon_{BB} = 0$), and the compressibility parameter $\kappa' = \beta \kappa_H v = 12.0$. This value of the compressibility parameter corresponds to approximately 3–5% of fluctuations in the total density. The same holds for the noise. The noise and compressibility are important for creating the physically realistic model, and we have discussed their effect on phase separation in detail earlier [27,29]. The new dimensionless parameter $\tilde{\gamma}$ for the shear is chosen equal to $\tilde{\gamma} = \Delta t \dot{\gamma} = 10^{-3}$, the same value as used in [1]. The dimensionless parameters allow us to apply results to different

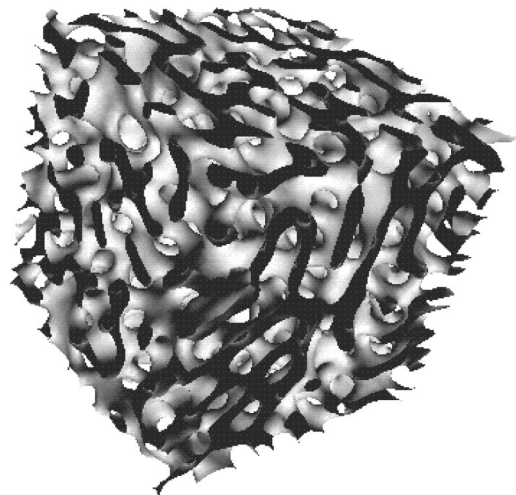


FIG. 6. Isosurface representation of the A_8B_8 melt at $\tau=4000$ with diffusion only. The isosurface is $v_A \rho_A = 0.3$.

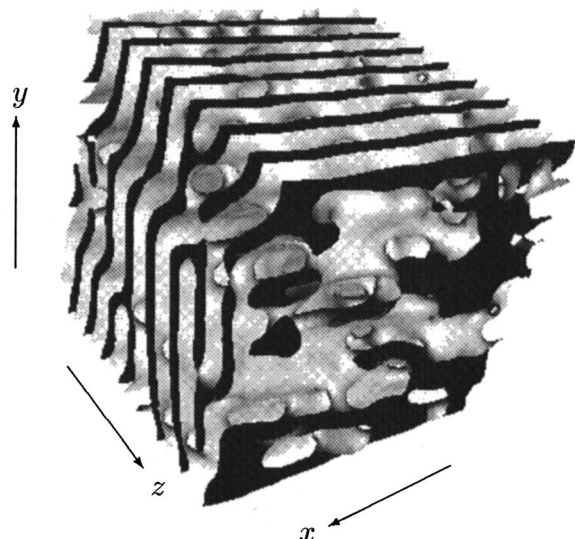


FIG. 7. Isosurface representation of the A_8B_8 melt at $\tau=4000$ and shear flow $v_x = \dot{\gamma}y$, $v_y = v_z = 0$, using the structure at $\tau=500$ (Fig. 5) as a starting structure. The isosurface is $\nu_{AP_A} = 0.3$.

systems. For example, for typical diffusion coefficient $\beta^{-1}M \sim 10^{-14} - 10^{-13} \text{ m}^2\text{s}^{-1}$ the shear rate is $\dot{\gamma} \sim 10 - 10^2 \text{ s}^{-1}$.

In Fig. 1 the results of the simulation in 2D ($L=128$) are shown. From $\tau=0$ (homogeneous melt) to $\tau=500$ [Fig. 1(a)] no shear is applied. At $\tau=500$, in the stage of an already well developed meso-phase structure, steady simple shear is initiated. In the early stages of shearing [Fig. 1(b)] clusters of lamellae inclined to the flow direction appear. In later stages the lamellae reorient themselves almost parallel to the flow direction [Figs. 1(c) and 1(d)]. At $\tau=4000$ the external flow was removed. The morphology pattern of almost perfect parallel lamellae remains stable and structure defects slowly disappear due to diffusion [Fig. 1(e)]. The picture differs completely from the phase separation pattern in the absence of shear [Fig. 1(f)], which consists of many local (lamellar) clusters without any global orientation. The morphology formation can be illustrated by the volume averaged factor $Q = \langle \nabla_x \rho \nabla_y \rho \rangle_V$ (Fig. 2), which is a measure of the spatial anisotropy of the domains distorted by the shear flow [18] and is related to the stress tensor [3,35]. In case of perfect lamellae parallel to the shear direction $Q=0$. The increase of Q from $\tau=0$ to 500 corresponds to the formation of more and more sharp boundaries. Without shear (top line) Q reaches a plateau region very soon after $\tau=500$. The decrease of the factor Q (bottom line) in case of shear describes reorientation of lamellae. Q becomes slightly negative as the lamellae align at a small angle to the shear direction. The process of reorientation from inclined to parallel lamellae is demonstrated on slices of the density pattern of the same run at more frequent time intervals (Figs. 3 and 4). Different structural changes such as undulation of lamellae, breakup, and recombination can be clearly observed. The process consists of defect formation and breakup, which is followed by recombination of pieces of lamellae from neighboring layers (Fig. 3). In Fig. 4 one can easily see that shear speeds up the defect disappearance in almost perfectly oriented lamellae.

Then we performed a 3D simulation ($L=64$) of the same system at the same shear rate as in Fig. 1. The initial struc-

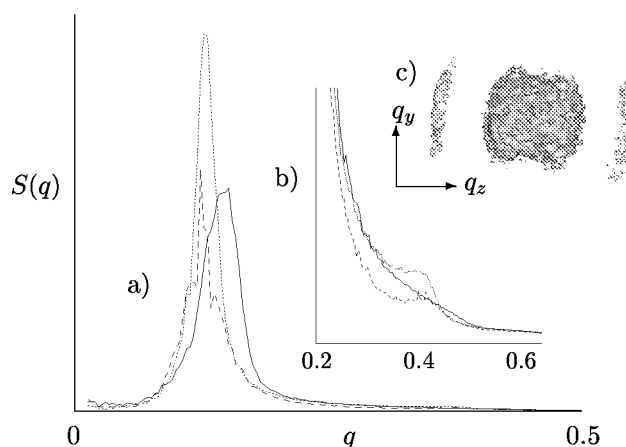


FIG. 8. Three-dimensional structure factor $S(\mathbf{q})$ (c) of the lamellae in Fig. 7, and the direction averaged structure factors $S(q)$ (a) and (b) of structures in Fig. 5 (solid line), 6 (dotted line), and 7 (dashed line). Fig. (b) is the shoulder part of Fig. (a) magnified in ordinate direction.

ture at $\tau=500$ (Fig. 5) has a lot of defects. During the application of steady simple shear between $\tau=500$ and 4000 a global lamellar orientation appears (Fig. 7) with few defects. The picture essentially differs from one without shear (Fig. 6), where only a few local lamellar clusters with many defects can be found. Hence application of shear speeds up lamellar formation in a diblock polymer melts enormously. The alignment qualitatively differs from the 2D case: so-called “perpendicular” lamellae are formed in 3D. From experiments and stability analysis this orientation is well known to be the most stable one [2,5,6]. As can be concluded from Fig. 2 lamellae formation and alignment is slower in 3D than in 2D.

The central peak and the peak at multiple frequency of the structure factor $S(\mathbf{q})$ [Fig. 8(c)] clearly indicate the lamellar pattern on Fig. 7. The shape of higher order peaks reflects both the deviation of lamellar orientation from the perfect order and the presence of defects. The small tilt of the whole picture also indicates that the alignment to the flow direction is not yet completely perfect. The shift of the central peak to the lower frequencies [Fig. 8(a)] during time evolution of averaged structure factor $S(q)$ demonstrates creation of larger structures. The third order peak is clearly observed [Fig. 8(b)] but the second one is still hidden inside the wide shoulder of the central peak.

We emphasize, that as we have shown in [24], our method cannot be reduced to earlier theories based on Landau Hamiltonian since it involves the calculation of the full polymer path integral. Our approach can be used for investigation of shear induced ordering in *specific* polymer systems. For example, the simulation of morphology evolution of Pluronic water mixtures [33] (lamellar, hexagonal, micellar, and bicontinuous phases) under shear is in progress. For the case of other lamellar orientations, for example, at slow shear rate, we expect that the viscous effects become important [36] and one should use a hydrodynamic description [2,3] instead of diffusion-convection with a given velocity field. Such analysis is also in progress.

A.V.Z. and G.J.A.S. acknowledge the support of the ESPRIT project MESODYN project No. ESPRIT EP22685 of the European Community.

- [1] H. Kodama and M. Doi, *Macromolecules* **29**, 2652 (1996).
- [2] G. H. Fredrickson, *J. Rheol.* **38**, 1045 (1994).
- [3] A. Onuki, *J. Phys. Condens. Matter* **9**, 6119 (1997).
- [4] B. Schmittmann and R. K. P. Zia, in *Phase Transitions and Critical Phenomena*, edited by C. Domb and J. Lebowitz (Academic, London, 1994).
- [5] Z.-R. Chen, J. A. Kornfield, S. D. Smith, J. T. Grothaus, and M. M. Sattkowski, *Science* **277**, 1248 (1997).
- [6] M. Goulian and S. T. Milner, *Phys. Rev. Lett.* **74**, 1775 (1995).
- [7] C.-Y. Huang and M. Muthukumar, *J. Chem. Phys.* **107**, 5561 (1997).
- [8] P. D. Olmsted and C.-Y. D. Lu, *Phys. Rev. E* **56**, R55 (1997).
- [9] M. E. Cates and S. T. Milner, *Phys. Rev. Lett.* **62**, 1856 (1989).
- [10] N. P. Balsara and H. J. Dai, *J. Chem. Phys.* **105**, 2942 (1996).
- [11] I. W. Hamley, K. A. Koppi, J. F. Rosedale, F. S. Bates, K. Almdal, and K. Mortensen, *Macromolecules* **26**, 5959 (1993).
- [12] H. Wang, P. K. Kesani, N. P. Balsara, and B. Hammouda, *Macromolecules* **30**, 982 (1997).
- [13] D. A. Hajduk, T. Tepe, H. Takenouchi, M. Tirrel, F. S. Bates, K. A. Almdal, and K. Mortensen, *J. Chem. Phys.* **108**, 326 (1998).
- [14] Z.-R. Chen, A. M. Issaian, J. A. Kornfield, S. D. Smith, J. T. Grothaus, and M. M. Sattkowski, *Macromolecules* **30**, 7096 (1997).
- [15] D. Qiwei He and E. B. Nauman, *Chem. Eng. Sci.* **52**, 481 (1997).
- [16] G. Gonnella, E. Orlandini, and J. M. Yeomans, *Phys. Rev. Lett.* **78**, 1695 (1997).
- [17] G. Pätzold and K. Dawson, *J. Chem. Phys.* **104**, 5932 (1996).
- [18] T. Ohta, H. Nozaki, and M. Doi, *Phys. Lett. A* **145**, 304 (1990).
- [19] S. Komura and J.-I. Fukuda, *Phys. Lett. A* **208**, 108 (1995).
- [20] H. Kodama and S. Komura, *J. Phys. II* **7**, 7 (1997).
- [21] J. W. Cahn and J. E. Hilliard, *J. Chem. Phys.* **28**, 258 (1958).
- [22] Y. Oono and S. Puri, *Phys. Rev. Lett.* **58**, 836 (1987).
- [23] P. G. de Gennes, *J. Chem. Phys.* **72**, 4756 (1980).
- [24] N. M. Maurits and J. G. E. M. Fraaije, *J. Chem. Phys.* **106**, 6730 (1997).
- [25] J. G. E. M. Fraaije, *J. Chem. Phys.* **99**, 9202 (1993).
- [26] J. G. E. M. Fraaije, B. A. C. van Vlimmeren, N. M. Maurits, M. Postma, O. A. Evers, C. Hoffmann, P. Altevogt, and G. Goldbeck-Wood, *J. Chem. Phys.* **106**, 4260 (1997).
- [27] N. M. Maurits, B. A. C. van Vlimmeren, and J. G. E. M. Fraaije, *Phys. Rev. E* **56**, 816 (1997).
- [28] N. M. Maurits and J. G. E. M. Fraaije, *J. Chem. Phys.* **107**, 5879 (1997).
- [29] B. A. C. van Vlimmeren and J. G. E. M. Fraaije, *Comput. Phys. Commun.* **99**, 21 (1996).
- [30] N. M. Maurits, P. Altevogt, O. A. Evers, and J. G. E. M. Fraaije, *Comput. Polym. Sci.* **6**, 1 (1996).
- [31] T. Kawakatsu, *Phys. Rev. E* **56**, 3240 (1997).
- [32] R. Hasegawa and M. Doi, *Macromolecules* **30**, 3086 (1997).
- [33] B. A. C. van Vlimmeren, N. M. Maurits, A. V. Zvelindovsky, G. J. A. Sevink, and J. G. E. M. Fraaije (unpublished).
- [34] M. Doi and D. Chen, *J. Chem. Phys.* **90**, 5271 (1989).
- [35] N. M. Maurits, A. V. Zvelindovsky, and J. G. E. M. Fraaije, *J. Chem. Phys.* **108**, 2638 (1998).
- [36] N. M. Maurits, A. V. Zvelindovsky, G. J. A. Sevink, B. A. C. van Vlimmeren, and J. G. E. M. Fraaije, *J. Chem. Phys.* (to be published).